

Nanostructured Pr-doped Ceria (PCO) thin films as sensing electrodes in  
solid-electrolyte type gas sensors with enhanced toluene sensitivity

Taro Ueda<sup>1\*</sup>, Thomas Defferriere<sup>2</sup>, Takeo Hyodo<sup>1</sup>, Yasuhiro Shimizu<sup>1</sup>, Harry L. Tuller<sup>2,3</sup>

<sup>1</sup>Graduate School of Engineering, Nagasaki University,

1-14 Bunkyo-machi, Nagasaki 852-8521, Japan

<sup>2</sup>Department of Materials Science and Engineering, Massachusetts Institute of Technology,

77 Massachusetts Avenue, Cambridge, Massachusetts 02139, USA

<sup>3</sup>International Institute of Carbon Neutral Energy Research, Kyushu University,

744 Motooka, Nishi-ku, Fukuoka 819-0395, Japan

## **Abstract**

$\text{Pr}_{0.1}\text{Ce}_{0.9}\text{O}_2$  (PCO) films, with columnar structure containing voids, were fabricated by pulsed laser deposition (PLD) and integrated into YSZ-based potentiometric gas sensor as a sensing electrodes (SEs). Sensors with PCO film thicknesses of 550, 1100 and 2200 nm, fabricated by controlling the number of PLD shots of 750, 1500 and 3000 respectively, were examined over the temperature range of 450–600°C. The sensor output voltage,  $E$ , of all sensors showed increasing negative change with increasing toluene concentration. The sensor with the thickest PCO SE film (thickness: 2200 nm) showed a much larger toluene response at 450°C than the others (PCO-SE thickness: 550, 1100 nm). Because PCO is a mixed ionic and electronic conductor and the morphology of SE was porous, the electrochemical oxidation reaction is viewed as occurring at the double phase boundaries – DPBs (interfaces between PCO/gas) as well as triple phase boundaries – TPBs (interfaces of PCO/YSZ/gas). Because a fraction of the toluene is catalytically oxidized in part during gas diffusion within the SE films, especially at lower operating temperatures, the much larger toluene response can be explained by the electrochemical oxidation reaction of the partially oxidized products together with toluene at the TPBs and DPBs.

***Keywords:*** *solid-electrolyte gas sensor, YSZ, pulsed laser deposition, (Pr,Ce)O<sub>2</sub>, toluene*

## 1 Introduction

The exhaled breath of patients suffering from lung cancer, diabetes and periodontitis contains higher concentration of toluene, acetone and hydrogen sulfide, respectively, than that of healthy individuals. [1, 2]. While the solid-electrolyte type gas sensor, compared to various other kinds of gas sensors, is an attractive candidate for the sensitive detection of such gases, further optimization of their sensing electrodes (SEs) with respect to their compositions and/or structures, remains an important objective [3–9]. We previously reported that the addition of CeO<sub>2</sub> to the Au SE, applied to yttria-stabilized zirconia (YSZ)-based solid electrolyte gas sensors, increased their toluene response [10]. Generally, the VOC-sensing mechanism of solid-electrolyte type gas sensors is explained on the basis of the mixed potential theory [11]. The electrochemical oxidation of toluene (Eq. (1)) and electrochemical reduction of oxygen (Eq. (2)) are expected to proceed simultaneously at the same rate at the triple phase boundaries (TPBs) located at the region of the SE in contact with the YSZ.



We previously confirmed that the addition of CeO<sub>2</sub> to the Au SE enhances electrochemical toluene oxidation activity on the basis of current-voltage (*I-E*) measurements. Therefore, we concluded that enhanced toluene oxidation activity is indispensable for increased toluene response. Recently, researchers reported that an increase in the triple phase boundary length (TPBL), the boundary at which the SE, YSZ and gas intersect, improved sensor response [12–14]. Sun et al. increased the TPBL by roughing the YSZ surface by sand blasting with SiC, thereby the NO<sub>2</sub> response of an YSZ-based gas sensor with a NiO SE increased by 150% [12]. However, no quantitative studies between the TPBL and sensor response were presented. We have focused instead on the use of mixed ionic and electronic conductors (MIECs) as SE materials to increase the concentration of gas-reaction sites. Recently, Bishop et al. reported that the addition of Pr to CeO<sub>2</sub> leads to significant increases in mixed ionic and

electronic conductivity in CeO<sub>2</sub> under oxidizing conditions [15, 16]. This was attributed to the relative ease in reducing Pr from the 4+ valence state, isovalent with Ce<sup>4+</sup>, to the 3+ valence state, leading to the introduction of both positively charged oxygen vacancies and small polaron electrons, leading in turn, to MIEC. The optimum level of Pr substitution was reported to be 10 mol%. This provided for relatively high levels of MIEC, as well as resistance to cracking observed at higher Pr levels due to increasing degrees of chemical expansion. Swallow et al. prepared thin Pr-doped CeO<sub>2</sub> films with a thickness of ca. 1000 nm by pulsed laser deposition (PLD), and evaluated the films' thermo- and chemo-mechanical properties by subjecting the films to temperature and oxygen partial pressure variations [17]. Film morphologies prepared by PLD were reported to be impacted by oxygen partial pressure utilized during ablation, with increased oxygen partial pressure resulting in well-developed porous structures [18–20].

In this study, we fabricated 10 mol% Pr-doped CeO<sub>2</sub> (Pr<sub>0.1</sub>Ce<sub>0.9</sub>O<sub>2</sub>, PCO) films with controlled thickness (550–2200 nm) by PLD, and investigated the toluene-sensing properties of YSZ-based sensors utilizing PLD grown PCO films as SEs. The effects of PCO SE thickness on toluene response were evaluated and discussed in terms of the DPBs and TPBs associated with the gas-reaction sites.

## **2 Experimental**

### **2.1 Fabrication of PCO thin film**

The PCO target (2.5 cm in diameter) was fabricated from PCO powder prepared through a co-precipitation process described briefly below [21]. A solution of praseodymium and cerium in the stoichiometric proportion (10/90) was prepared by dissolving praseodymium nitrate Pr(NO<sub>3</sub>)<sub>3</sub>·6H<sub>2</sub>O and cerium nitrate Ce(NO<sub>3</sub>)<sub>3</sub>·6H<sub>2</sub>O (Strem Chemicals), in distilled water to reach a concentration of 0.1 mol/L. An ammonium carbonate aqueous solution (0.5 mol/L) was added dropwise into this

solution. The amount of ammonium carbonate solution was calculated to have a molar excess of 2.5 as compared to the total amount of cations in the nitrate solution. The obtained precipitate was filtered and washed four times in distilled water. After drying in an oven at 100°C, the as-obtained powder was fired at 600°C for 4 h in flowing air. The dense PCO target (density: 97%) was then prepared by isostatic pressing PCO powder (1000 kgf/cm<sup>2</sup>) at room temperature followed by sintering at 1500°C for 6 h in air.

The films were deposited onto polished single crystal wafers of YSZ (ZrO<sub>2</sub> with 8 mol% Y<sub>2</sub>O<sub>3</sub>, MTI, orientation: (001)) by PLD (Surface systems+technology) using a 248 nm KrF excimer laser with pulse energy of 150 mJ at a repetition rate of 2, 5 or 10 Hz at a heater temperature of 250°C. After evacuation below  $1 \times 10^{-3}$  Pa, oxygen was introduced into the deposition chamber to attain an oxygen background pressure of 1.3 or 30 Pa. The obtained films were denoted as PCO ( $p,f,x$ ) ( $p$ : oxygen partial pressure (1.3 or 30 Pa),  $f$ : Pulse repetition rate (2, 5 or 10 Hz),  $x$ : shot number (750, 1500 or 3000)). The films were structurally characterized by high-resolution X-ray diffraction with Cu K $\alpha_1$  radiation (Rigaku, SmartLab) and atomic force microscopy (AFM, Bruker, Dimension 3100). The secondary electron images of the films were obtained by scanning electron microscopy (SEM; Carl Zeiss, MERLIN).

## 2.2 Fabrication of sensors and measurement of toluene-sensing properties

The fabricated PCO film was used as a sensing electrode (SE), with a Pt paste (Engelhard) brushed onto the backside of the YSZ substrate to serve as the counter electrode (CE, 4 mm  $\times$  8 mm). After annealing at 900°C for 2 h in air, planar-type YSZ-based gas sensors, denoted as SE/YSZ/CE sensors (SE: PCO ( $p,f,x$ ), CE: Pt) were obtained.

The gas-sensing properties of the sensors were examined by measuring the open circuit voltage between the two electrodes ( $E$ , mV) in air or in 0.25–50 ppm toluene balanced with dry air, under a gas-flow rate of 200 cm<sup>3</sup> min<sup>-1</sup> at temperatures of 450, 500, 550 and 600°C. The sensor output voltage,  $E$ , was measured with a digital electrometer (Keysight Technologies, 34970A). The magnitude of the

sensor response ( $\Delta E$ ) was defined as the difference between  $E$  measured in toluene balanced with dry air and that in dry air.

### 3 Results and discussions

Figure 1 shows cross-sectional SEM images of the PCO thin films. Film growth was strongly influenced by the PLD chamber oxygen partial pressure (see Fig. 1 (a)). PCO (1.3,5,3000) showed a dense structure and had a thickness of ca. 300 nm while PCO (30,5,3000) exhibited a columnar structure with a 4 times larger film thickness than that of PCO (1.3,5,3000). Though YSZ and PCO are both body-centered cubic lattices with closely matching lattice constants, at sufficiently low temperatures ( $<500^{\circ}\text{C}$ ), it is expected that PCO would grow by nucleation, growth and island coalescence [22]. Infortuna et al. explained that the presence of an ambient gas limited plume expansion, leading to an increase in collisions amongst the emitted particles [23]. This would result in an increased nucleation density and growth of clusters, consistent with the higher degree of granularity of PCO (30,5,3000) compared to those of PCO (1.3,5,3000). Schneider et al. discussed how the first nucleated subcritical clusters tend to dissociate into mobile species that nucleate new clusters with different size during PLD. If atoms do not have sufficient time or mobility to dissociate and re-agglomerate before the next pulse is shot, then the structure will develop abnormal grains and porosity [24]. This appears to be consistent with the fact that for our samples, the temperature is sufficiently high ( $250^{\circ}\text{C}$  during the PLD process), and the deposition process is sufficiently slow, for the deposited clusters to partially dissociate and agglomerate prior to the accumulation of other clusters atop them (see Fig.1 (a)(i)). On the other hand, the increase in the pulse repetition rate from 5 Hz to 10 Hz, increased the film thickness and resulted in a well-developed columnar structure (see Fig. 1 (b)(ii)). From a nucleation theory based argument, Schneider et al. discussed how increasing the repetition rate will increase the degree of supersaturation of the evaporated material on the surface of the substrate,

and that will impact the density of the first nucleated subcritical clusters. With limited thermal energy to enable atom redistribution, and a shorter time in between pulses, this will result in a more granular and porous structure. Porous and columnar structures offer ready gas penetration into the films. As a consequence, 10 Hz and 30 Pa were selected in this study as appropriate pulse repetition rate and oxygen pressure, respectively. The porous PCO films with different thicknesses were also prepared by controlling the shot number. The film thickness increased proportionally with shot number, while maintaining the columnar structure. Film thicknesses of 550 nm and 1100 nm were obtained by using shot numbers of 750 and 1500, respectively (see Fig. 1 (c)). Figure 2 (a) and (b) show AFM images of the surface of PCO (30,10,750) and PCO (30,10,3000). The roughness of PCO (30,10,3000) (ca. 13.8 nm) was larger than that of PCO (30,10,750) (ca. 8.69 nm). This is probably due to the greater accumulation of PCO clusters onto the surfaces of the columnar PCO particles already deposited onto the YSZ substrate. Figure 2 (c) shows the XRD pattern of PCO (30,10,1500). The cubic phase of  $\text{Pr}_{0.1}\text{Ce}_{0.9}\text{O}_2$ , without preferred orientations, was confirmed for the film grown on single crystal YSZ (001).

Figure 3 shows the response transients of the PCO (30,10,*x*)/YSZ/Pt sensors (*x*: 750, 1500, 3000) to toluene (5–50 ppm) at 450, 500, 550 and 600°C in dry air. Figure 4 shows variations in response of these sensors to 5 ppm and 50 ppm toluene in dry air with operating temperature. The *E* values of all sensors showed increasing negative polarity with increasing toluene concentration. The responses of the PCO (30,10,750)/YSZ/Pt and PCO (30,10,1500)/YSZ/Pt sensors were relatively small at 450°C, but their response increased with increasing operating temperature. On the other hand, the PCO (30,10,3000)/YSZ/Pt sensor showed much larger toluene response even at 450°C than the PCO (30,10,750)/YSZ/Pt and PCO (30,10,1500)/YSZ/Pt sensors, but, on the other hand, the response of the PCO (30,10,3000)/YSZ/Pt sensor to 5 ppm toluene decreased with increasing operating temperature. The response of the PCO (30,10,3000)/YSZ/Pt sensor to 50 ppm toluene was the largest at 500°C, and

the response to 50 ppm toluene increased with increasing PCO SE thickness over the whole temperature range examined. Ultimately, the response of the PCO (30,10,3000)/YSZ/Pt sensor became smaller than those of the PCO (30,10,750)/YSZ/Pt and PCO (30,10,1500)/YSZ/Pt sensors when exposed to 5 ppm toluene at 600°C.

Generally, the triple phase boundaries (TPBs – the interfaces of PCO/YSZ/gas) serve as the gas-reaction sites operative for toluene response in solid-electrolyte type gas sensors. The electrochemical oxidation of toluene at these sites largely affects the magnitude of the toluene response as described in the introduction. The electrochemical oxidation of toluene increases with increasing operating temperature, and correspondingly the response of the PCO (30,10,750)/YSZ/Pt and PCO (30,10,1500)/YSZ/Pt sensors increased with increasing operating temperature. However, a certain fraction of the toluene is catalytically oxidized to H<sub>2</sub>O and CO<sub>2</sub> during diffusion from the SE surface to the YSZ/SE interface, leading to a decreased concentration of toluene arriving at the TPBs. Figure 5 shows a schematic view of the elements that influence toluene response with increased PCO thickness. The percentage of catalytic toluene oxidation increased with an increase in the thickness of PCO SE. The catalytic activity for toluene oxidation also increased with increasing operating temperature, thereby leading to a decrease in the toluene concentration arriving at the TPBs. Therefore, it is likely that high catalytic activity of toluene oxidation over PCO resulted in the smaller toluene response of the PCO (30,10,3000)/YSZ/Pt sensor at 600°C than those at lower temperatures.

In this study, the PCO mixed ionic and electronic conductor was used as the SE material. In addition, given that the morphology of the SE films was porous (see Fig. 1), electrochemical reactions at the double phase boundaries (DPBs – the interfaces between PCO/gas) in the PCO SE need also be considered. This is particularly the case, given that the double phase boundary area (DPBA) associated with the PCO columnar structure should be much larger than the TPBL in terms of the concentration of active reaction sites. The toluene response increased with an increase in the thickness of SE. This supports the key contribution of the DPBs to an increase in toluene response. The increased DPBA,

achieved by increasing PCO SE thickness, was also found to be more effective in increasing the toluene response than the increased amount of catalytic toluene oxidation during gas diffusion in the SE films at temperatures less than 550°C.

In addition, it should also be noted that a certain amount of toluene can be catalytically oxidized in part during gas diffusion within the SE films, especially at lower operating temperatures. Cao et al. reported that the partially oxidized products of toluene were benzaldehyde ( $C_6H_5CHO$ ) and benzoic acid ( $C_6H_5COOH$ ) [25]. In this study, the SE films exhibited a columnar structure containing voids with a film thickness ranging from 550 to 2200 nm. Thus, the concentration of partially oxidized products should be highest as one approaches the bottom of the SE films, i.e. approaching the TPBs. In addition, the concentration of partially oxidized products is expected to increase with an increase in the PCO SE thickness. Therefore, the much larger toluene response of the PCO (30,10,3000)/YSZ/Pt sensor at 450°C than that of the PCO (30,10,750)/YSZ/Pt sensor can be explained by the electrochemical oxidation reaction of the partially oxidized products together with toluene at the TPBs and DPBs as gas-reaction sites, although the catalytic oxidation of toluene simultaneously proceeds during gas diffusion within the SE films. On the other hand, the response to 5 ppm toluene of the PCO (30,10,3000)/YSZ/Pt sensor at 600°C was smaller than that of the PCO (30,10,750)/YSZ/Pt sensor, probably due to high catalytic activity of toluene oxidation at higher temperature.

In order to separate the contribution of partially oxidized products to toluene response from the contribution of DPBs, the SE-thickness dependence of the PCO (30,10,x)/YSZ/Pt sensors to 500 ppm CO was examined at 450, 500, 550 and 600°C in air, as shown in Fig. 6. The PCO (30,10,3000)/YSZ/Pt sensor showed much smaller responses to CO than the ones to 50 ppm toluene at the examined temperature range, which indicated the selective toluene response of the sensor versus CO. In addition, the magnitude of the CO response increased with an increase in the thickness of the PCO SE, at 450, 500 and 550°C. However, the difference in CO response between the PCO (30,10,3000)/YSZ/Pt sensor and the PCO (30,10,750)/YSZ/Pt sensor at 450°C was much smaller than that of the toluene response.

Generally, CO simply reacts with oxygen species on the PCO to produce only CO<sub>2</sub>. Since the actual concentration of CO at the TPBs and the DPBs decreases with an increase in thickness of the SE films due to the catalytic oxidation of CO during the gas diffusion in the SE films, this confirms that the DPBs contribute to the sensor response together with the TPBs. In addition, it was also found that the larger toluene response of the PCO (30,10,3000)/YSZ/Pt sensor at 450°C than that of the other sensors was probably due to the electrochemical oxidation of partially oxidized products of toluene at the TPBs and DPBs. On the other hand, the smaller CO response of the PCO (30,10,3000)/YSZ/Pt sensor than that of the PCO (30,10,*x*)/YSZ/Pt sensors (*x*: 750, 1500) at 600°C was probably due to the catalytic CO oxidation during gas diffusion in the SE films. Namely, the actual concentration of CO at the TPBs and the DPBs became lower, because the catalytic activity of metal oxides for CO oxidation increases with increasing temperatures.

Figure 7 shows the toluene concentration dependences of the PCO (30,10,1500)/YSZ/Pt and PCO (30,10,3000)/YSZ/Pt sensors in the lower concentration range (0.25–5 ppm) at 500°C. The PCO (30,10,3000)/YSZ/Pt sensor showed a much larger toluene response than that of the PCO (30,10,1500)/YSZ/Pt sensor. These sensors showed an almost linear relationship between *E* and the logarithm of toluene concentration, although the *E* of the PCO (30,10,3000)/YSZ/Pt sensor to 0.25 ppm toluene did not fit the linear dependence. This is probably due to a larger amount of partial toluene oxidation during gas diffusion in the case of low concentration of toluene than the case of higher concentration. Thus, a further increase in the PCO-SE thickness could increase the toluene response by increasing the fraction of partially oxidized products, together with the contribution of the increasing DPBA. The PCO (30,10,3000)/YSZ/Pt sensor could detect concentrations as low as 0.25 ppm (ca. -26.5 mV).

Table 1 summarizes typical examples of toluene detection using solid-electrolyte type gas sensors. We found an appropriate selection of composition and structure of SE is one of key factors achieving large toluene response. Zosel et al. reported a Nb<sub>2</sub>O<sub>5</sub>-added Au SE, which was fabricated by a screen-

printing technique, was effective in detecting toluene sensitively [10]. We also clarified an addition of CeO<sub>2</sub> to a Au SE largely increased the toluene response [26]. On the other hand, pristine oxide SEs mixed without noble metal such as Au have also been shown as a promising candidate for toluene detection [8, 9, 29–33]. Especially, Sato et al. demonstrated that a sensor attached with a NiO SE, fabricated by application of a NiO paste on YSZ, detected a low concentration of toluene (0.01 ppm) [8, 9]. The sensors using the CeO<sub>2</sub>-added Au SE [10] or the NiO SE [8, 9] showed larger toluene response than the PCO (30,10,3000)/YSZ/Pt sensor, even though the electrochemical toluene oxidation of their reference sensors proceeded on only the TPBs. One of a possible reason is that gas diffusivity in the SEs of their reference sensors was much higher than that of the PCO (30,10,3000)/YSZ/Pt sensor, because the porosity in the SEs of their reference sensors was much larger than that of the PCO (30,10,3000)/YSZ/Pt sensor. The easy gas diffusion in the SEs of their reference sensors resulted in a high concentration of toluene around the TPBs at the YSZ/SE interface regardless of their large SE thicknesses (ca. 10–15 μm). As an example of sensors using thin-film SEs, Mori et al. fabricated a Pt SE (thickness: ca. 15 nm) on YSZ by a magnetron sputtering method, and the sensor showed large response to 0.5 ppm toluene (ca. –71 mV) by a Au lamination on the Pt SE [27, 28]. In the case of the PCO SE in this study, the electrochemical oxidation of toluene and/or the partially oxidized products proceeds on the DPBs as well as on the TPBs. However, the density of each columnar PCO microstructure (diameter: ca. 100 nm) which constitutes the PCO SE is relatively large, and thus toluene cannot easily diffuse inside the columnar PCO microstructures. Therefore, the toluene diffusivity inside the columnar PCO microstructures is much lower than that from the surface of the PCO SE to the bottom (namely, the YSZ/SE interface with the TPBs). This indicates that a large number of DPBs inside the columnar PCO microstructures does not sufficiently contribute as the active electrochemical-oxidation sites of toluene and/or the partially oxidized products, even for the PCO (30,10,3000)/YSZ/Pt sensor. Based on the discussions above, it's greatly expected that the morphological optimization (e.g., the diameter and the porosity of the columnar PCO microstructures,

and the size of the PCO crystallites) by strictly controlling the PLD conditions and the subsequent treatments drastically improve the toluene response.

#### 4. Conclusions

PCO thin films (PCO ( $p,f,x$ )) were fabricated on single crystal YSZ by the PLD method, and the toluene-sensing properties of PCO ( $30,10,x$ )/YSZ/Pt sensors were measured in the temperature range of 450–600°C. PCO ( $1.3,5,3000$ ) showed a dense structure, but PCO ( $30,5,3000$ ) exhibited a columnar structure and 4 times larger thickness than that of PCO ( $1.3,5,3000$ ). In addition, the increase in the pulse repetition rate from 5 Hz to 10 Hz increased the thickness and resulted in a well-developed columnar structure. The PCO thickness was successfully controlled from 550 to 2200 nm while maintaining its columnar structure.

The response of the PCO ( $30,10,x$ )/YSZ/Pt sensors ( $x$ : 750, 1500 and 3000) to 50 ppm toluene increased with an increase in PCO SE thickness, and the PCO ( $30,10,3000$ )/YSZ/Pt sensor showed a much larger response than those of the PCO ( $30,10,x$ )/YSZ/Pt sensors ( $x$ : 750, 1500) especially at the lower operating temperature of 450°C. This is attributed to the contribution of the electrochemical oxidation of toluene together with the partially oxidized products at the TPBs and DPBs. The PCO ( $30,10,3000$ )/YSZ/Pt sensor could detect concentrations of toluene as low as 0.25 ppm at 500°C. Based on these results, an increase in the length of the gas reaction pathway for the electrochemical oxidation of toluene appears to be indispensable for the enhancement of toluene response of solid-electrolyte type gas sensors.

*Acknowledgements:* This study was supported, in part, by the Promotion Program for Strategic International Research Network for accelerating Brain Circulation from the Japan Society for the Promotion of Science (JSPS). T.U. thanks the Tuller group at MIT for hosting his visit during the time the experimental studies were being performed. T.D., and H.L.T, acknowledge support for their research from the Department of Energy, Basic Energy Sciences under award number DE-SC0002633 (Chemomechanics of Far-From-Equilibrium Interfaces). This work made use of the MRSEC Shared Experimental Facilities at MIT, supported by the National Science Foundation.

Table 1

Sensor structure SE/Solid electrolyte/CE	Fabrication technique of SE	SE thickness / $\mu\text{m}$	Appropriate operating temperature / $^{\circ}\text{C}$	Detection range / $\text{ppm}$	Toluene response / $\text{mV}$	Year	Ref.
Au+Nb <sub>2</sub> O <sub>5</sub> /YSZ/Pt	Screen printing	10	700	0–4000	–85.0 (10 ppm)	2004	26
Au+CeO <sub>2</sub> /YSZ/Pt	Screen printing	10	400	0.5–50	–55.0 (0.5 ppm)	2017	10
NiO/YSZ/Pt	Application	No data	450	0.01–0.150	–17.0 (0.05 ppm)	2010	8
SnO <sub>2</sub> -coated NiO/YSZ/Pt	Application	15	450	0.01–0.3	–16.1 (0.05 ppm)	2013	9
La <sub>0.8</sub> Sr <sub>0.2</sub> CrO <sub>3</sub> /YSZ/Pt	Sintered compact	No data	520	1–4*	–6.9 (0.5 ppm)	2014	27
Zn <sub>3</sub> V <sub>2</sub> O <sub>8</sub> /YSZ/Pt	Application	No data	600	50, 100	–7.4 (50 ppm)	2015	28
NiNb <sub>2</sub> O <sub>6</sub> /YSZ/Pt	Application	No data	650	50	–5.8 (50 ppm)	2016	29
Co <sub>0.5</sub> Zn <sub>0.5</sub> Fe <sub>2</sub> O <sub>4</sub> /YSZ/Pt	Application	No data	650	50	–13.5 (50 ppm)	2018	30
Sr <sub>2</sub> FeMoO <sub>6</sub> /GDC <sup>†</sup> /Pt	Application	No data	590	20, 100	–21.6 (50 ppm)	2019	31
Pt/YSZ/Pt	Sputtering	No data	400	0.5–10	–15.1 (0.5 ppm)	2009	32
Au-coated Pt/YSZ/Pt	Sputtering	0.015	400	0.5–10	–69.3 (0.5 ppm)	2012	33
PCO/YSZ/Pt	PLD	2.2	500	0.25–50	–26.5 (0.25 ppm) –43.7 (0.5 ppm)		This study

\*Mixture of 6 kinds of VOCs  
<sup>†</sup>GDC: Gadolinium-doped ceria

## References

- [1] W.-T. Koo, S.-J. Choi, N.-H. Kim, J.-S. Jang, I.-D. Kim, Catalyst-decorated hollow WO<sub>3</sub> nanotubes using layer-by-layer self-assembly on polymeric nanofiber templates and their application in exhaled breath sensor, *Sens. Actuators B*, 223 (2016) 301–310.
- [2] K. Yaegaki, K. Sanada, Volatile sulfur compounds in mouth air from clinically healthy subjects and patients with periodontal disease, *J. Periodont. Res.*, 27 (1992) 233–238.
- [3] F. Liu, Y. Guan, R. Sun, Mixed potential type acetone sensor using stabilized zirconia and M<sub>3</sub>V<sub>2</sub>O<sub>8</sub> (M: Zn, Co and Ni) sensing electrode, *Sens. Actuators B*, 221 (2015) 673–680.
- [4] F. Liu, X. Yang, B. Wang, Y. Guan, X. Liang, P. Sun, G. Lu, High performance mixed potential type acetone sensor based on stabilized zirconia and NiNb<sub>2</sub>O<sub>6</sub> sensing electrode, *Sens. Actuators B*, 229 (2016) 200–208.
- [5] F. Liu, B. Wang, X. Yang, X. Liang, P. Sun, X. Chuai, Y. Gao, F. Liu, G. Lu, Sub-ppm YSZ-based mixed potential type acetone sensor utilizing columbite type composite oxide sensing electrode, *Sens. Actuators B*, 238 (2017) 928–937.
- [6] F. Liu, C. Ma, X. Hao, C. Yang, H. Zhuc, X. Liang, P. Sun, F. Liu, X. Chuai, G. Lu, Highly sensitive gas sensor based on stabilized zirconia and CdMoO<sub>4</sub> sensing electrode for detection of acetone, *Sens. Actuators B*, 248 (2017) 9–18.
- [7] M. Mori, Y. Itagaki, Y. Sadaoka, S. Nakagawa, M. Kida, T. Kojima, Detection of offensive odorant in air with a planar-type potentiometric gas sensor based on YSZ with Au and Pt electrodes, *Sens. Actuators B*, 191 (2014) 351–355.
- [8] T. Sato, V. V. Plashnitsa, M. Utiyama, N. Miura, Potentiometric YSZ-based sensor using NiO sensing electrode aiming at detection of volatile organic compounds (VOCs) in air environment, *Electrochem. Commun.*, 12 (2010) 524–526.

- [9] T. Sato, M. Breedon, N. Miura, Reduction in Ethanol Interference of Zirconia-Based Sensor for Selective Detection of Volatile Organic Compounds, *J. Electrochem. Soc.*, 160 (9) (2013) B146–B151.
- [10] T. Ueda, H. Abe, K. Kamada, S. R. Bishop, H. L. Tuller, T. Hyodo, Y. Shimizu, Enhanced sensing response of solid-electrolyte gas sensors to toluene: Role of composite Au/metal oxide sensing electrode, *Sens. Actuators B*, 252 (2017) 268–276.
- [11] N. Miura, T. Sato, S. Anggraini, H. Ikeda, S. Zhuiykov, A review of mixed-potential type zirconia-based gas sensors, *Ionics*, 20 (2014) 901–925.
- [12] R. Sun, Y. Guan, X. Cheng, Y. Guan, X. Liang, J. Ma, P. Sun, Y. Sun, G. Lu, High performance three-phase boundary obtained by sand blasting technology for mixed-potential-type zirconia-based NO<sub>2</sub> sensors, *Sens. Actuators B*, 210 (2015) 91–95.
- [13] X. Liang, S. Yang, J. Li, H. Zhang, Q. Diao, W. Zhao, G. Lu, Mixed-potential-type zirconia-based NO<sub>2</sub> sensor with high-performance three-phase boundary, *Sens. Actuators B*, 158 (2011) 1–8.
- [14] Y. Guan, C. Li, X. Cheng, B. Wang, R. Sun, X. Liang, J. Zhao, H. Chen, G. Lu, Highly sensitive mixed-potential-type NO<sub>2</sub> sensor with YSZ processed using femtosecond laser direct writing technology, *Sens. Actuators B*, 198 (2014) 110–113.
- [15] S. R. Bishop, T. S. Stefanikw, H. L. Tuller, Electrical conductivity and defect equilibria of Pr<sub>0.1</sub>Ce<sub>0.9</sub>O<sub>2-σ</sub>, *Phys. Chem. Chem. Phys.*, 13 (2011) 10165–10173.
- [16] S. R. Bishop, T. S. Stefanikw, H. L. Tuller, Defects and transport in Pr<sub>x</sub>Ce<sub>1-x</sub>O<sub>2-d</sub>: Composition trends, *J. Mater. Res.*, 27(15) (2012) 2009–2016.
- [17] J. G. Swallow, J. J. Kim, M. Kabir, J. F. Smith, H. L. Tuller, S. R. Bishop, K. J. V. Vliet, Operando reduction of elastic modulus in (Pr, Ce)O<sub>2-d</sub> thin films, *Acta Materialia*, 105 (2016) 16–24.
- [18] W. C. Chueh, Y. Hao, W. Jung and S. M. Haile, High electrochemical activity of the oxide phase in model ceria–Pt and ceria–Ni composite anodes, *Nature Mater.*, 11 (2012) 155–161.

- [19] E. M. Preiß, A. Krauß, V. Kekkonen, N. Barsan, H. Seidele, Characterization of WO<sub>3</sub> thin films prepared by picosecond laser deposition for gas sensing, *Sens. Actuators B*, 248 (2017) 153–159.
- [20] J. Huotari, V. Kekkonen, T. Haapalainen, M. Leidinger, T. Sauerwald, J. Puustinen, J. Liimatainen, J. Lappalainen, Pulsed laser deposition of metal oxide nanostructures for highly sensitive gas sensor applications, *Sens. Actuators B*, 236 (2016) 978–987.
- [21] L. Spiridigliozzi, G. Dell'Agli, A. Marocco, G. Accardo, M. Pansini, S. Yoon, H. Ham, D. Frattini, Engineered co-precipitation chemistry with ammonium carbonate for scalable synthesis and sintering of improved Sm<sub>0.2</sub>Ce<sub>0.8</sub>O<sub>1.90</sub> and Gd<sub>0.16</sub>Pr<sub>0.04</sub>Ce<sub>0.8</sub>O<sub>1.90</sub> electrolytes for IT-SOFCs, *J. Ind. Eng. Chem.*, 59 (2018) 17–27.
- [22] S. Cho, J. Yoon, J.-H. Kim, X. Zhang, A. Manthiram, H. Wang, “Microstructural and electrical properties of Ce<sub>0.9</sub>Gd<sub>0.1</sub>O<sub>1.95</sub> thin film electrolyte in solid oxide fuel cells” *J. Mater. Res.*, 26 (2011) 854–859.
- [23] A. Infortuna, A. S. Harvey, L. J. Gauckler “Microstructures of CGO and YSZ thin films by pulsed laser deposition” *Adv. Funt. Mater.*, 18 (2008) 127–135.
- [24] C. W. Schneider, T. K. M. Lippert “Laser ablation and thin film deposition” *Laser Processing of Materials* Edited by S. Peter, Springer (2010) 89–112.
- [25] L. Cao, Z. Gao, S. L. Suib, T. N. Obee, S. O. Hay, J. D. Freihaut, Photocatalytic oxidation of toluene on nanoscale TiO<sub>2</sub> catalysts: studies of deactivation and regeneration, *J. Catal.*, 196 (2000) 253–261.
- [26] J. Zosel, K. Ahlborn, R. Muller, D. Westphal, V. Vashook, U. Guth, Selectivity of HC-sensitive electrode materials for mixed potential gas sensors, *Solid State Ionics*, 169 (2004) 115–119.
- [27] P. K. Sekhar, K. Subramaniam, Detection of harmful Benzene, Toluene, Ethylbenzene, Xylenes (BTEX) vapors using electrochemical gas sensors, *ECS Electrochem. Lett.*, 3 (2) B1-B4 (2014).

- [28] F. Liu, Y. Guan, R. Sun, X. Liang, P. Sun, F. Liu, G. Lu, Mixed potential type acetone sensor using stabilized zirconia and  $M_3V_2O_8$  (M: Zn, Co and Ni) sensing electrodes, *Sens. Actuators B*, 221 (2015) 673–680.
- [29] F. Liu, X. Yang, B. Wang, Y. Guan, X. Liang, P. Sun, G. Lu, High performance mixed potential type acetone sensor based on stabilized zirconia and  $NiNb_2O_6$  sensing electrode, *Sens. Actuators B*, 229 (2016) 200–208.
- [30] X Hao, B. Wang, C. Ma, F. Liu, X. Yang, T. Liu, X. Liang, C. Yang, H. Zhu, G. Lu, Mixed potential type sensor based on stabilized zirconia and  $Co_{1-x}Zn_xFe_2O_4$  sensing electrode for detection of acetone, *Sens. Actuators B*, 255 (2018) 1173–1181.
- [31] T. Liu, W. Li, Y. Zhang, X. Hao, Y. Zhang, X. Liang, F. Liu, F. Liu, X. Yan, Y. Gao, T. Zhang, C. Zhang, G. Lu, Acetone sensing with a mixed potential sensor based on  $Ce_{0.8}Gd_{0.2}O_{1.95}$  solid electrolyte and  $Sr_2MMoO_6$  (M: Fe, Mg, Ni) sensing electrode, *Sens. Actuators B*, 284 (2019) 751–758
- [32] M. Mori, H. Nishimura, Y. Itagaki, Y. Sadaoka, E. Traversa, Detection of sub-ppm level of VOCs based on a Pt/YSZ/Pt potentiometric oxygen sensor with reference air, *Sens. Actuators B*, 143 (2009) 56–61.
- [33] M. Mori, Y. Itagaki, Y. Sadaoka, VOC detection by potentiometric oxygen sensor based on YSZ and modified Pt electrodes, *Sens. Actuators B*, 161 (2012) 471–479.

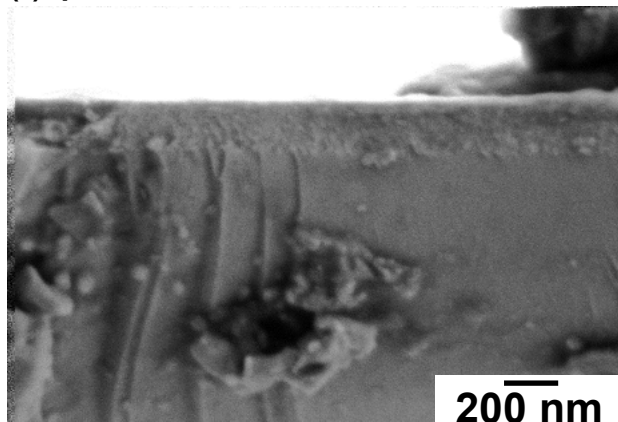
### **Figure captions**

- Fig. 1. Cross-sectional SEM images of PCO thin films (PCO ( $p,f,x$ )) deposited at 250°C.
- Fig. 2. (a, b) 3D views of non-contact mode AFM images of PCO (30,10,750) and PCO (30,10,3000) deposited at 250°C and (c) XRD spectra of PCO (30,10,1500) deposited onto single crystal YSZ.
- Fig. 3. Response transients of PCO (30,10, $x$ )/YSZ/Pt ( $x$ : 750, 1500, 3000) sensors to 5–50 ppm toluene at 450, 500, 550, 600°C in dry air.
- Fig. 4. Variations in response of the PCO (30,10, $x$ )/YSZ/Pt ( $x$ : 750, 1500, 3000) sensors to 5 ppm and 50 ppm toluene with operating temperature in dry air.
- Fig. 5. Schematic view of the elements influencing toluene response with increased PCO thickness.
- Fig. 6. Variations in response of PCO (30,10, $x$ )/YSZ/Pt ( $x$ : 750, 1500, 3000) sensors to 500 ppm CO in dry air as a function of SE thickness .
- Fig. 7. Concentration dependence of toluene response of the PCO (30,10, $x$ )/YSZ/Pt ( $x$ : 1500, 3000) sensors in dry air at 500°C.
- Table 1. Typical examples of toluene detection using solid-electrolyte type gas sensors.

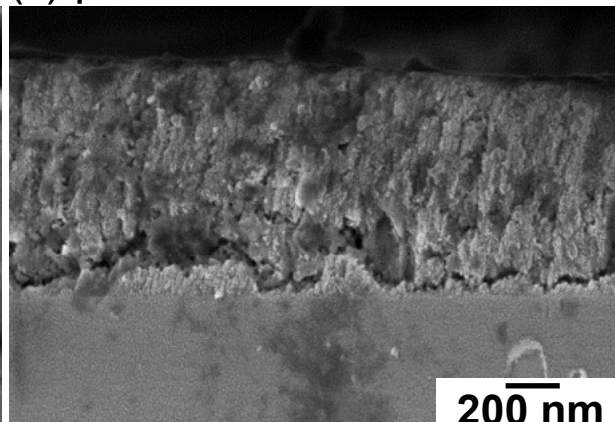
Fig. 1

(a) PCO ( $p, 5, 3000$ )

(i)  $p: 1.3$

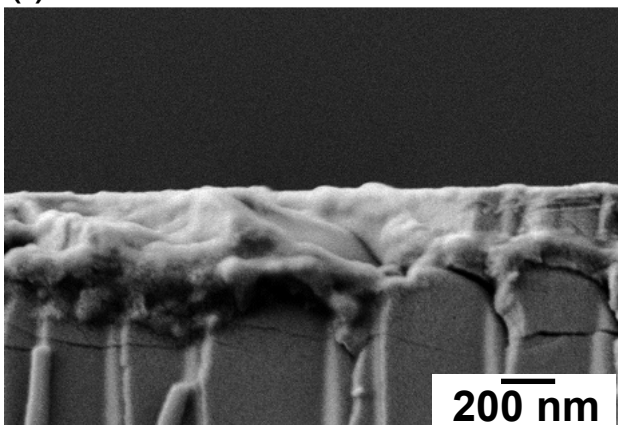


(ii)  $p: 30$

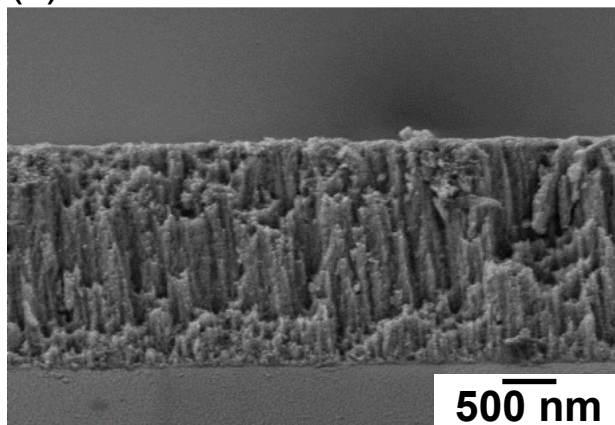


(b) PCO ( $30, f, 3000$ )

(i)  $f: 2$

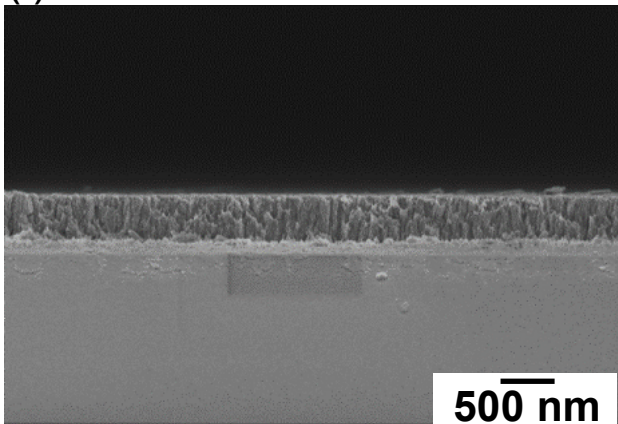


(ii)  $f: 10$



(c) PCO ( $30, 10, x$ )

(i)  $x: 750$



(ii)  $x: 1500$

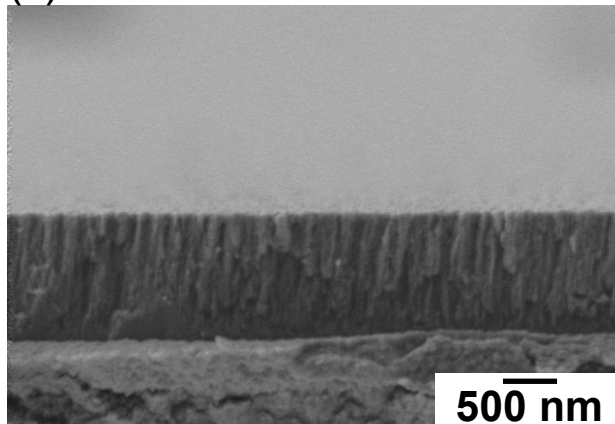
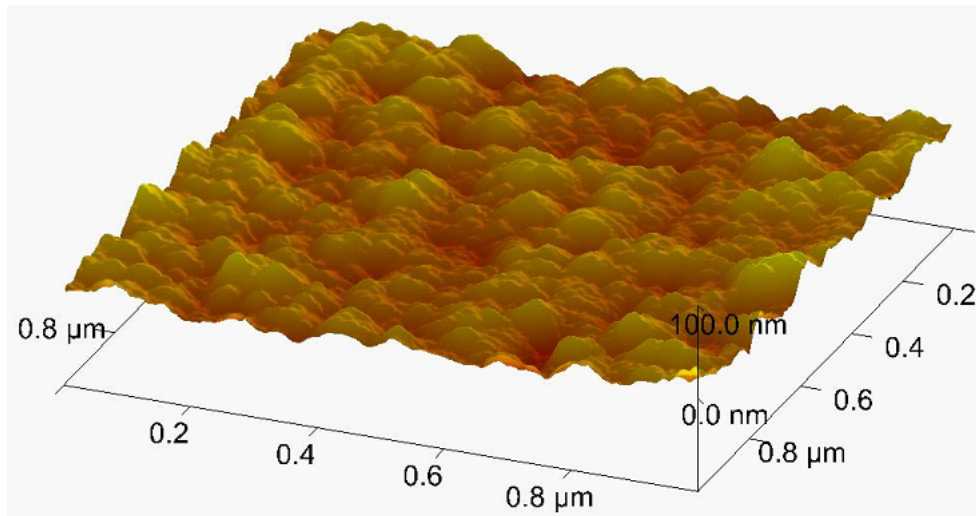


Fig. 2

(a) PCO (30,10,750)



(b) PCO (30,10,3000)

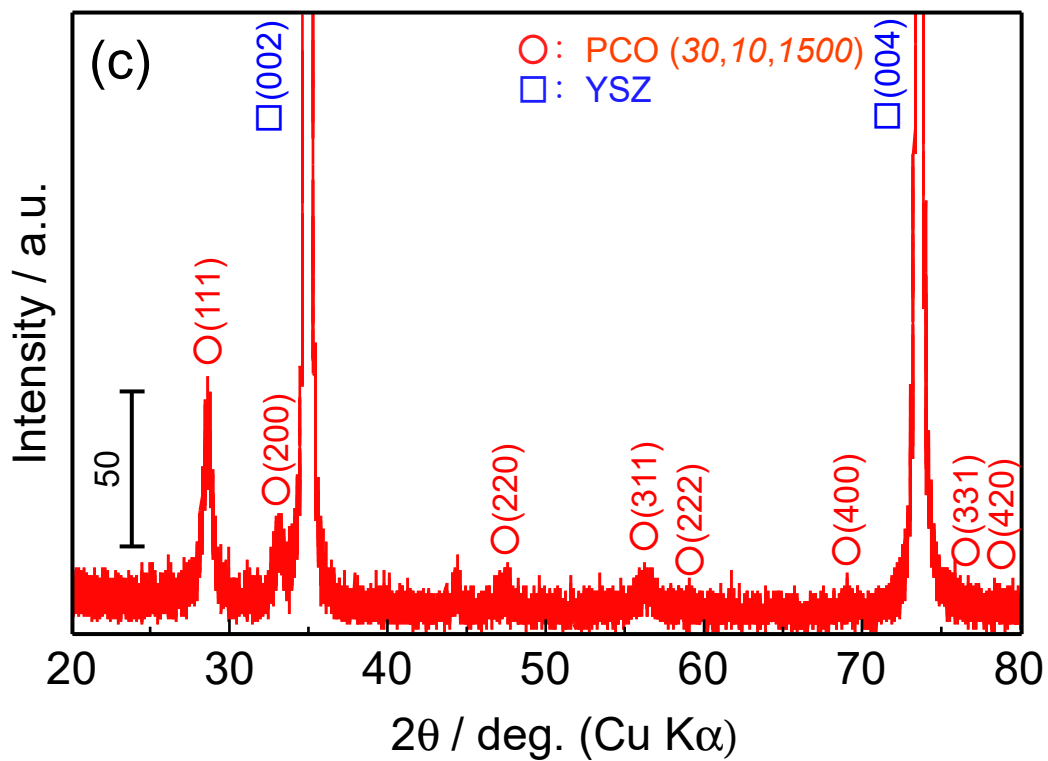
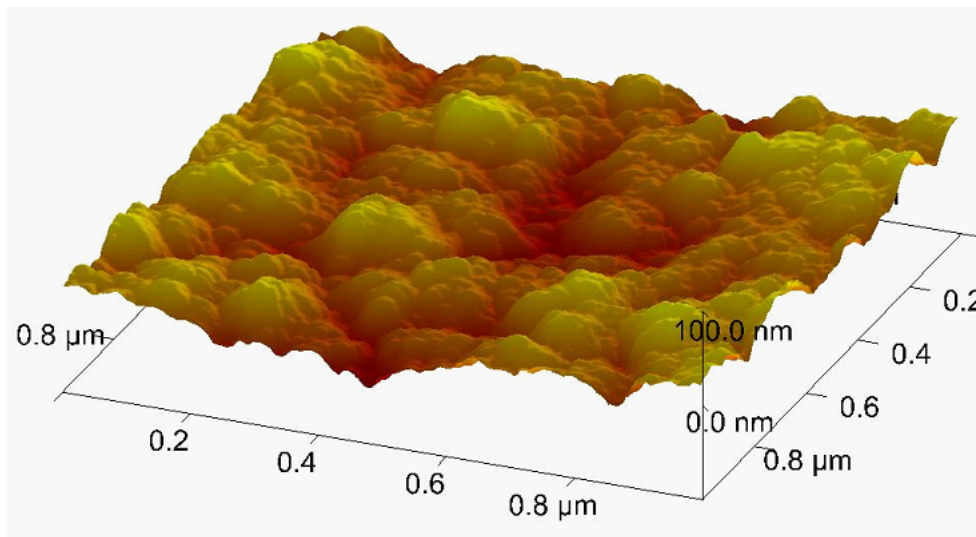


Fig. 3

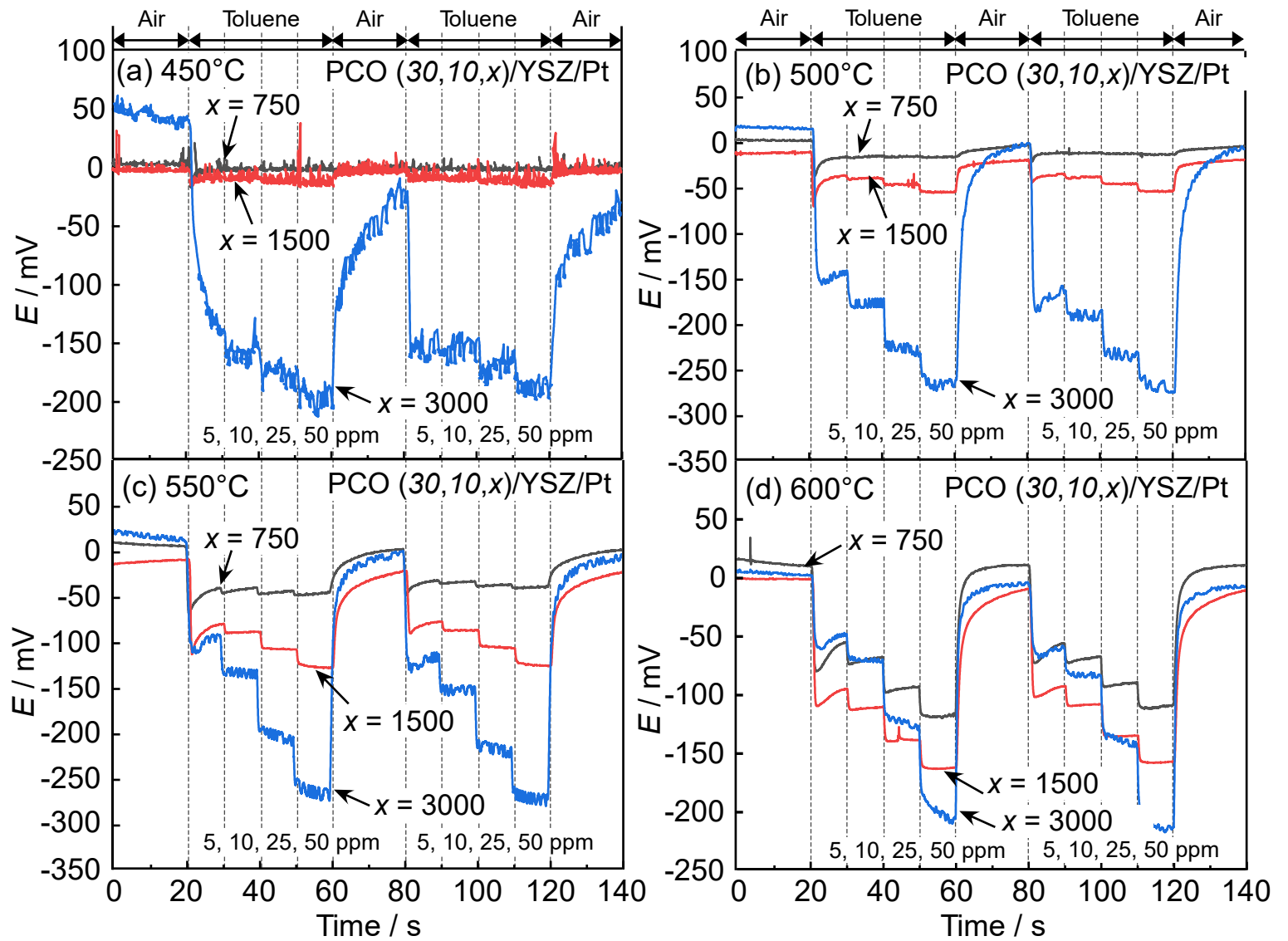


Fig. 4

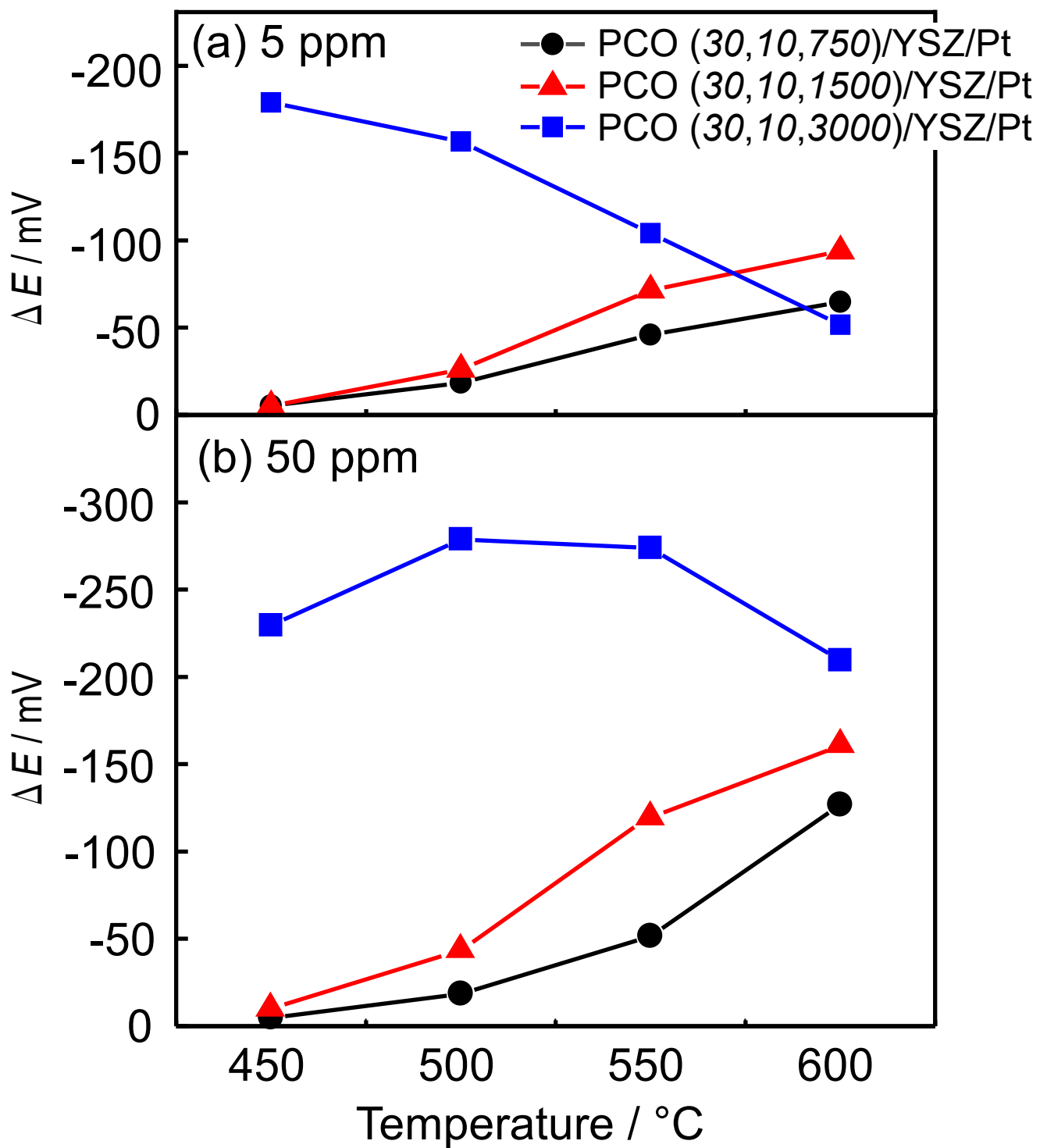


Fig. 5

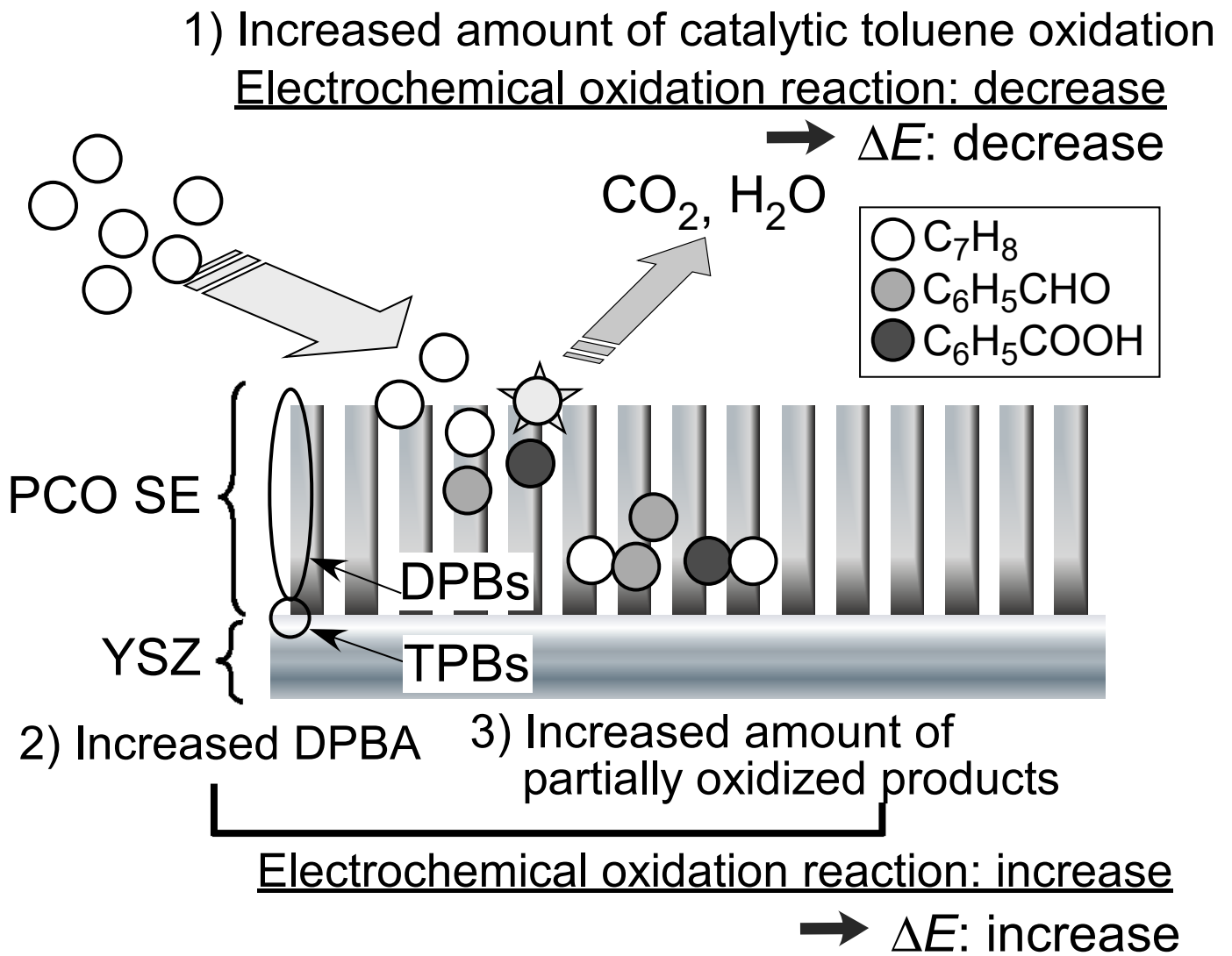


Fig. 6

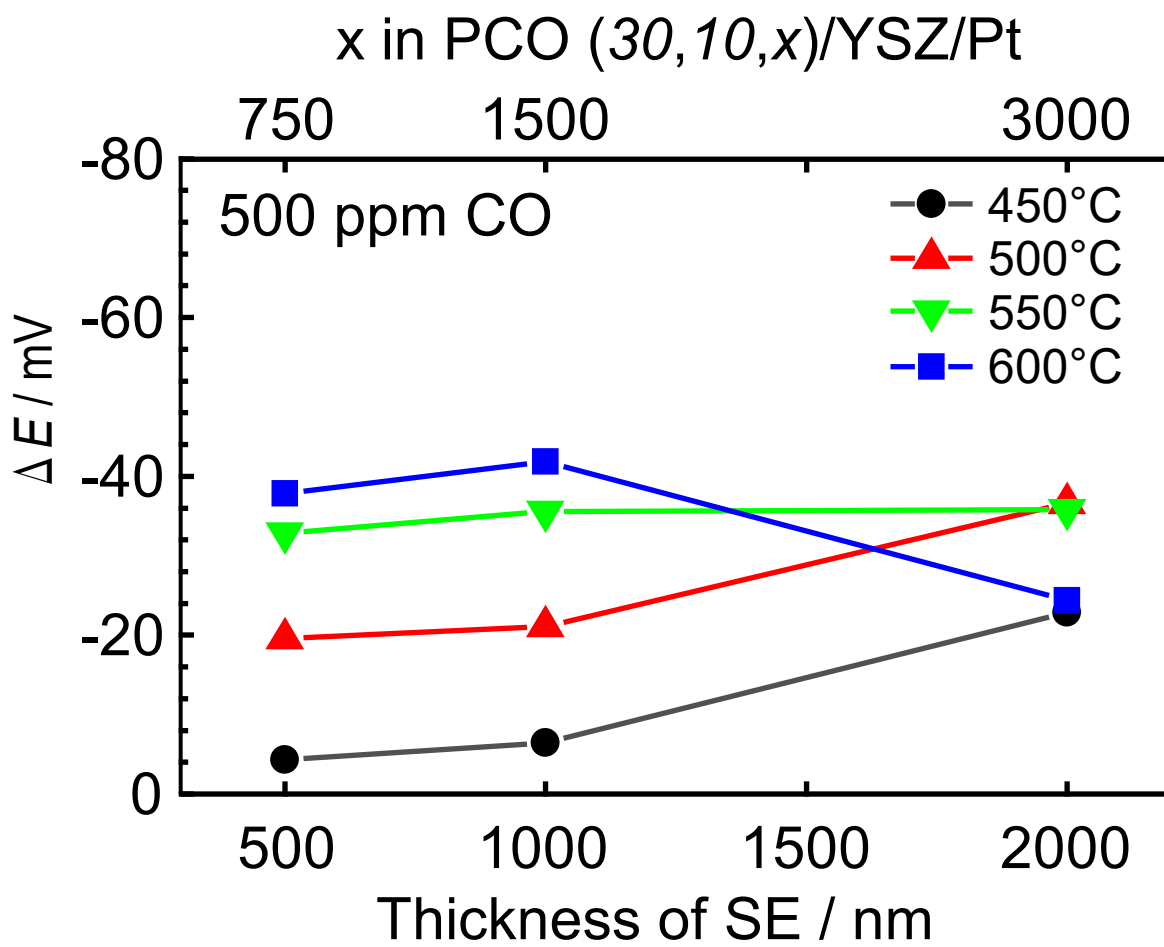


Fig. 7

